

ICONN 2015 [4th - 6th Feb 2015]**International Conference on Nanoscience and Nanotechnology-2015**
SRM University, Chennai, India

Structural and magnetic properties of heavily-doped Co into ZnO single crystals

P.P. Murmu^{1,2}, J. Kennedy^{1,2*}¹National Isotope Centre, GNS Science, PO Box 31312, Lower Hutt 5010, New Zealand²The MacDiarmid Institute for Advanced Materials and Nanotechnology, New Zealand

Abstract: We present the structural, morphological and magnetic properties of low-energy Co doped and annealed ZnO single crystals. Dynamic-TRIM calculations predict a mean projected range of 10-16 nm resulting in Co concentration of 12-24 atomic % in the surface layer of ZnO. Rutherford backscattering spectrometry in channeling condition (RBS/C) revealed that the Co implanted ZnO remains partially crystalline even for the highest fluence of 1×10^{17} ions cm^{-2} . Raman spectroscopy results showed a broad implantation induced disorder from 520 to 600 cm^{-1} along with a peak from $A_1(\text{LO})$ mode of ZnO. A secondary phase observed in XRD is attributed to the Cobalt oxide. AFM analysis showed cluster formation at the surface in the Co implanted ZnO single crystals annealed at 700 °C for 60 min. under high vacuum. SQUID measurements at 5 K of Co ion implanted and annealed samples exhibited ferromagnetic properties.

Keywords: Structural, magnetic properties, doped Co, ZnO single crystals.

Introduction

Dilute magnetic semiconductors (DMSs) have attracted significant attention due to their potential application in spintronic devices. Mn doped GaAs remained the most understood DMS system where spin polarization between magnetic moment is established by delocalized holes¹. Since the prediction of room temperature ferromagnetism in zinc oxide (ZnO) based DMS systems, Co doped ZnO (ZnO:Co) was intensively studied. Co doped ZnO has been a potential candidate due to its large solubility into the host matrix. Various solubility limits have been reported in the literature²⁻⁴. Different growth techniques have been used to fabricate the Co:ZnO films such as radio-frequency (rf) magnetron sputtering⁵, pulsed laser deposition (PLD)⁶, molecular beam epitaxy (MBE)⁷, sol-gel synthesis⁸ and ion implantation^{4,9}. The ion implantation technique is well-known method to introduce the dopant elements into the matrix of host substrates at desired depth and precise concentration. However, it may cause ion beam induced disorder, and subsequent annealing can lead to formation of Co secondary phases and the formation of super-paramagnetic clusters of consist of Zn, Co and O^{9,10}. Consistent observation of ferromagnetism in Co:ZnO remains elusive as the precipitation of secondary phases and nanocrystalline clusters can significantly influence the magnetic interactions in the material.

High-dose doping of ZnO has been attempted in order to understand the magnetic ordering mechanism in the material¹¹⁻¹³. Lee *et al*¹¹ performed first-principles spin-density functional calculations on Co doped ZnO

and found that high concentration of Co doping is necessary to establish the ferromagnetic ordering mediated by the electron carriers. However, Heo *et al.*¹² studied heavily doped Mn into ZnO and reported that the high concentration doping alone cannot result in ferromagnetic ordering which is significantly affected by the quality of the film and intrinsic defects. Moreover, high concentration doping has been shown to form metallic clusters and precipitation of secondary phases¹³. Additionally, annealing process may also affect the formation of metallic clusters and secondary phases altering the nature of magnetic ordering in the film¹⁴. Annealing is usually required in ion implanted films to recover their crystalline quality and activate the charge carriers¹⁵. In this paper, we present a study of low-energy Co ions implanted into ZnO single crystals with high-dose and subsequent annealing effects on their structural, morphological and magnetic properties. High-dose implantation and annealing appear to have significant contributions towards the precipitation of Co oxide (CoO) secondary phase.

Experimental

Co⁺ ions were doped into ZnO (0001) single crystals (Semiwafer Inc.) using the GNS Science ion implanter facility with ion energies between 20 and 40 keV[16]. DYNAMIC-TRIM¹⁷ calculations were performed to obtain the projected ion range and its concentrations into ZnO. The calculations give the projected range between 10 and 16 nm for fluences ranging from 2.6×10^{16} to 1.0×10^{17} ions cm⁻² resulting in Co concentrations of 12 to 24 atomic % at the surface layer. Annealing in a vacuum of better than 10^{-6} mbar was performed between 650 and 700 °C from 30 to 90 min. The ion beam analysis technique Rutherford backscattering spectrometry in channeling condition (RBS/C) was used to investigate the crystalline nature of Co implanted and annealed ZnO¹⁸. 2.0 MeV He⁺ ions impinged the samples under normal incidence with a typical current density of 15 nA cm⁻²¹⁹. The backscattered ions were measured by surface barrier detector placed at backscattering angle of 165°. Structural properties were examined by XRD using Cu K_α radiation and Raman spectroscopy. Raman spectroscopy measurements were conducted using Ar⁺ laser ($\lambda = 514$ nm) and the spectra were collected at backscattering geometry using liquid nitrogen cooled CCD. The surface morphology of Co implanted and annealed ZnO samples were analyzed with atomic force microscopy (AFM) in contact mode. A Superconducting Quantum Interference Device (SQUID) was used to carry out the magnetic measurements with the applied field parallel to the sample surface²⁰.

Results and Discussion

RBS/C was employed to study the crystalline quality of ZnO single crystals upon Co implantation and annealing. Figure 1 shows the random and [0001]-aligned RBS spectra for 2.6×10^{16} Co cm⁻² implanted and 650 °C annealed ZnO single crystals. The minimum yield (χ_{\min}), defined as the ratio of RBS backscattering yield in channeled to random conditions, for Zn is found to be around 55.2% which decreased to around 28.5% upon annealing the sample at 650 °C. For 1.0×10^{17} Co cm⁻² implanted and 700 °C annealed ZnO single crystal Zn minimum yield was found to be around 68%. The lower values of Zn minimum yields suggest that the layer is partially crystalline upon Co implantation and annealing. Similar trend was observed for ZnO implanted with heavier elements such as Gd[18] indicating high radiation tolerance of ZnO.

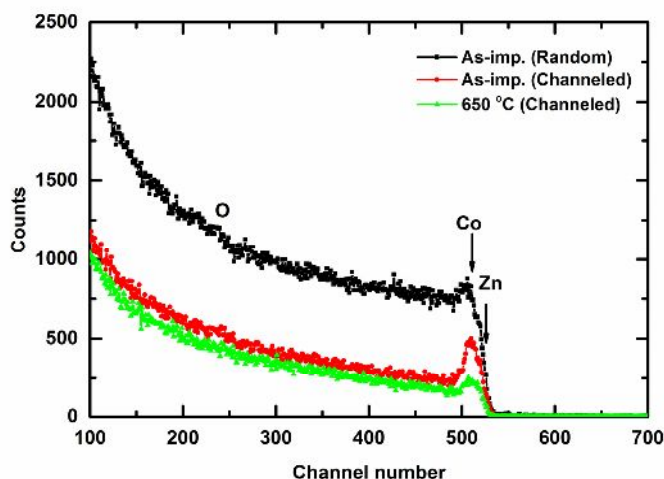


Fig. 1: Random and [0001]-aligned RBS spectra for 2.6×10^{16} Co cm⁻² implanted and 650 °C annealed ZnO single crystals.

Structural properties of Co implanted and annealed ZnO were investigated using Raman spectroscopy. Figure 2 illustrates the Raman spectra of 2.6×10^{16} Co cm^{-2} implanted and 650 °C annealed ZnO single crystals. Typical Raman peaks attributed to wurtzite ZnO were observed at around 438 cm^{-1} originating from $E_2(\text{high})$ mode. The $2E_2(\text{M})$ peaks were also observed in all the samples which are associated with the second order scattering in ZnO. Raman peak at around 576 cm^{-1} is attributed to the $A_1(\text{LO})$ mode of ZnO, which overlaps a broad peak from 520 to 600 cm^{-1} in as-implanted sample. The broad peak is significantly reduced upon annealing the sample at 650 °C for 30 min. Further annealing for longer duration (90 min.) had no additional impact suggesting annealing the sample at 650 °C for 30 min. was sufficient to recover the implantation induced disorders in ZnO. Similar behavior was also observed in rare-earth implanted ZnO single crystals [18]. Broad peaks in the 520 to 600 cm^{-1} region are often reported in ion implanted ZnO and they appear to match the phonon DOS in disordered ZnO^{21, 22}. Additionally, intrinsic defects such as oxygen vacancies are also shown to increase the Raman scattering from the whole Brillouin zone along with resonant Raman scattering which result in enhanced $A_1(\text{LO})$ peak²²

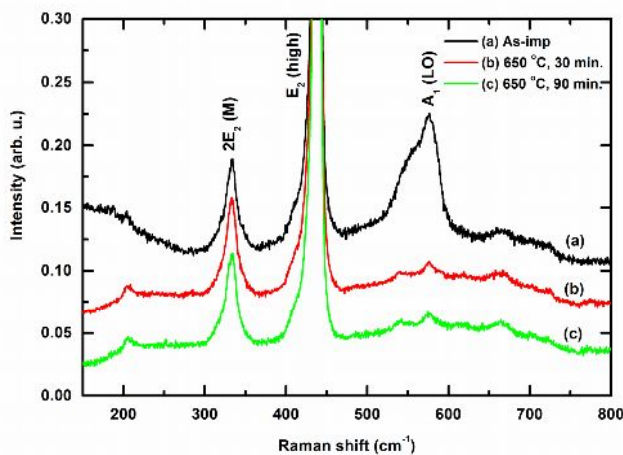


Fig. 2: Raman spectra of 2.6×10^{16} Co cm^{-2} implanted and 650 °C annealed ZnO single crystals.

X-ray diffraction was used to investigate the crystalline phase and the orientation. The X-ray diffraction pattern of 4.5×10^{16} and 1.0×10^{17} Co cm^{-2} implanted and 700 °C annealed ZnO single crystals are shown in Fig. 3. The major XRD peaks near 31.3 and 34.6° are associated with the reflection from (001) and (002) planes of ZnO²³. There is an additional XRD peak observed at around 42.7° for 1.0×10^{17} Co cm^{-2} implanted and annealed ZnO which is related to diffraction from (200) plane of CoO. No other peaks corresponding to Co and/or related complexes were observed. Moreover, ZnO XRD peak in 1.0×10^{17} Co cm^{-2} implanted and annealed ZnO was found to be shifted slightly towards the higher angle suggesting that the highest dose implantation and annealing resulted in a small compressive stress. The Scherrer formula, $d = 0.9\lambda / (\beta \cos\theta)$, where λ is the X-ray wavelength, θ the Bragg angle and β the FWHM of 2θ in radians, indicates a crystalline size of around 31.7 nm for 1.0×10^{17} Co cm^{-2} implanted and annealed ZnO.

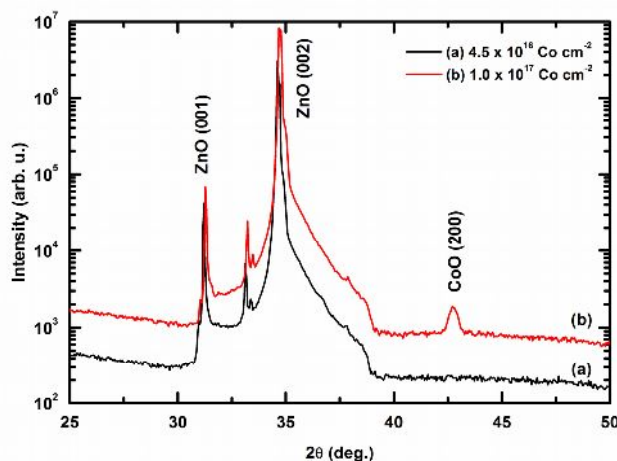


Fig. 3: XRD spectra of (a) 4.5×10^{16} and (b) 1.0×10^{17} Co cm^{-2} implanted and 700 °C annealed ZnO single crystals.

AFM analysis was performed to study the morphological alterations caused by the ion implantation process and the annealing procedure. The un-implanted ZnO surface is relatively smooth with root mean square (rms) surface roughness of 0.8 nm and upon Co implantation the rms value increases up to 1.4 nm. However, with annealing at 700 °C for 60 minutes the surface roughness increases up to 7.4 nm as shown in Fig. 4. The high dose implantation and annealing tend to enhance the coalescence of small grains to form bigger grains which results in the formation of Co clusters and/or secondary phases.

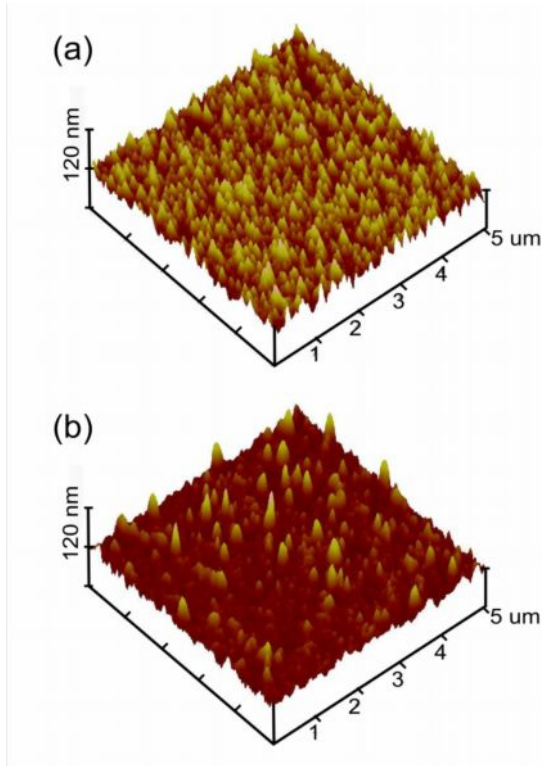


Fig. 4: AFM images of (a) 4.5×10^{16} and (b) 1.0×10^{17} Co cm⁻² implanted and 700 °C annealed ZnO single crystals.

Magnetic properties of Co implanted ZnO were studied using SQUID magnetometer. Figure 5 shows a representative field dependent magnetic moment curve obtained at 5 K for a 1.0×10^{17} Co cm⁻² implanted and 700 °C annealed ZnO single crystal. It is evident from the Fig. 5 that the sample showed ferromagnetic behavior. The curve gives a saturation magnetic moment of $0.38 \mu_B$ per implanted Co ion. If all the Co ions are in cluster form then the calculated magnetic moment per Co ion is 1.6 whereas the magnetic moment per ion of Co²⁺ in high spin state is $3 \mu_B$ /Co^{10, 24}. The low magnetic moment has been associated with anti-ferromagnetic coupling in Co-O-Co system²⁵. The anti-ferromagnetic coupling of CoO below 289 K²⁶ may contribute significantly to suppress the magnetic moment in ZnO:Co systems.

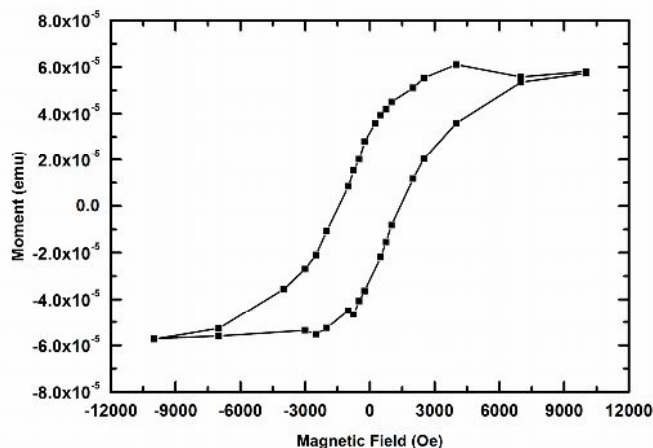


Fig. 5: M(H) curve for a 1.0×10^{17} Co cm⁻² implanted and 700 °C annealed ZnO single crystal.

Summary

We have investigated the structural, morphological and magnetic properties of Co ions implanted with high-dose into ZnO single crystals. RBS/C results revealed that high-dose doping of Co into ZnO still retains the partial crystalline quality suggesting high radiation resistance of ZnO. Raman spectroscopy results showed a broad peak around $A_1(LO)$ peak resulting from implantation induced disorders which is recovered upon annealing the sample. An XRD reflection from cobalt oxide CoO (200) planes was observed in the higher dose implanted and annealed sample which might arise from the oxidation of Co nanocrystals. AFM analysis reveals the formation of a nanostructured surface. A low magnetic moment per Co ion is observed which is attributed to antiferromagnetic coupling in Co-O-Co, Co nanoclusters and/or secondary phases.

Acknowledgements

We acknowledge funding from the Ministry of Business, Innovation and Employment, New Zealand (C05x0802 and C08x01206).

References:

1. Jungwirth T, Sinova J, et al.; Phys. Rev. B, 2007, 76: 125206.
2. Prellier W, Fouchet A, Mercey B, Simon C, et al., Appl. Phys. Lett., 2003, 82: 3490.
3. Ueda K, Tabada H, and Kawai T, Appl. Phys. Lett., 2001, 79: 988.
4. Akdogan N, Nefedov A, Westerholt K, Zabel H, et al., J. Phys. D: Appl. Phys., 2008, 41, 165001.
5. Lim S W, Hawang S K, and Myoung J M, Solid State Commun., 2003, 125: 231.
6. Yan L, Ong C K and Rao X S, J. Appl. Phys., 2004, 96: 508.
7. Jin Z, Fukumura T, Kawasaki M, et al., Appl. Phys. Lett., 2001, 78: 3824.
8. Lee H J, Jeong S Y, Cho C R, et al., Appl. Phys. Lett., 2002, 81: 155202.
9. Zhou S, Potzger K, Von Borany J, Grotzschel R, et al., Phys. Rev. B, 2008, 77: 035209.
10. Potzger K, Zhou S, Xu Q, Shalimov A, et al., Appl. Phys. Lett., 2008, 93: 232504.
11. Lee E-C, and Chang K J, Phys. Rev. B, 2004, 69: 085205.
12. Heo Y W, Ivill M P, Ip K, et al., Appl. Phys. Lett., 2004, 84: 2292-2294.
13. Schumm M, Koerdel M, Müller S, et al., J. Appl. Phys., 2009, 1105: 083525.
14. Potzger K, Kuepper K, Xu Q, et al., J. Appl. Phys., 2008, 104: 023510.
15. Chen B, Tang K, et al., Appl. Surf. Sci., 2014, 313: 152-158.
16. Kennedy J, Murmu P P, et al., J. Alloy Comp., 2014, 616: 614-617.
17. Biersack J P, Nucl. Instr. and Meth. B, 1987, 27: 21.
18. Murmu P P, Mendelsberg R J, et al.; J. Appl. Phys., 2011, 110: 033534.
19. Christie V A, Liem S I, et al., Curr. Appl. Phys., 2004, 4: 225-228.
20. Kennedy J, Leveneur J, et al., Nanotechnology, 2011, 22: 115602.
21. Schumm M, Koerdel M, Müller S, et al., New J. Phys., 2008, 10: 043004.
22. Chen Z Q, Kawasuso A, Xu Y, et al., J. Appl. Phys., 2005, 97: 013528.
23. Murmu P P, Kennedy J, Ruck B J, Markwitz A, Mater. Sci. For., 2012, 700: 49-52.
24. Patterson C H, Phys. Rev. B., 2006, 74: 144432.
25. Ney A, Ollefs K, Ye S, Kammaermeir T, et al., Phys. Rev. Lett., 2008, 100: 157201.
26. Silinsky P S, and Sehra M S, Phys. Rev. B, 1981, 24: 419-423.
